inorganics

MDPI

Article

Anti-Proliferative and Anti-Migration Activity of Arene–Ruthenium(II) Complexes with Azole Therapeutic Agents

Legna Colina-Vegas [1], Katia M. Oliveira [1], Beatriz N. Cunha [1,2], Marcia Regina Cominetti [3], Maribel Navarro [4,5,*] and Alzir Azevedo Batista [1,*]

1 Departamento de Química, Universidade Federal de São Carlos, CEP 13565-905 São Carlos, SP, Brazil; esleg_24@hotmail.com (L.C.-V.); kmoliveiraq@gmail.com (K.M.O.); beatriz.cunha@ifgoiano.edu.br (B.N.C.)
2 Instituto Federal Goiano—IFG, Campus Ceres, CEP 76300-00 Ceres, GO, Brazil
3 Departamento de Gerontologia, Universidade Federal de São Carlos, CEP 13565-905 São Carlos, SP, Brazil; mcominetti@ufscar.br
4 Instituto Nacional de Metrologia, Qualidade e Tecnologia, INMETRO, CEP 25250-020 Xerem, RJ, Brazil
5 Departamento de Química, ICE, Universidade Federal de Juiz de Fora, CEP 36036-900 Juiz de Fora, MG, Brazil
* Correspondence: maribel.navarro@ufjf.edu.br (M.N.); daab@ufscar.br (A.A.B.)

Received: 24 October 2018; Accepted: 5 December 2018; Published: 11 December 2018

Abstract: The efficacy of organoruthenium complexes containing ergosterol biosynthesis inhibitors (CTZ: clotrimazole, KTZ: ketoconazole and FCZ: fluconazole) against tumor cells, and their interaction with important macro-biomolecules such as human serum albumin and DNA have been investigated here. Our experimental results indicated that these ruthenium(II) complexes present spontaneous electrostatic interactions with albumin, and act as minor groove binders with the DNA. The ability of these Ru(II)–azole complexes to inhibit the proliferation of selected human tumor and non-tumor cell lines was determined by MTT assay. Complexes [RuCl(CTZ)(η^6-*p*-cymene)(PPh_3)]PF_6 (**3**) and [RuCl(KTZ)(η^6-*p*-cymene)(PPh_3)]PF_6 (**4**) were shown to be between 3- and 40-fold more cytotoxic than the free ligands and the positive control cisplatin. Complex **3** was selected to continue studies on the triple negative breast tumor cell line MDA-MB-231, inducing morphological changes, loss of adhesion, inhibition of colony formation, and migration through Boyden chambers, cell cycle arrest in the sub-G1 phase, and a mechanism of cell death by apoptosis. All these interesting results show the potential of this class of organometallic Ru(II) complexes as an antiproliferative agent.

Keywords: ruthenium complexes; antiproliferative; antimigration; DNA interaction; HSA binding

1. Introduction

According to the WHO, cancer is a generic term for a group of diseases involving abnormal cell growth with the potential to invade or spread to other parts of the body. There are over 100 different known cancer types that affect humans, causing about 8.2 million deaths, estimated as 13% of all deaths worldwide. In 2012, about 14.1 million new cases of cancer occurred globally (not including skin cancer other than melanoma) [1]. One of the principal causes of cancer deaths is the developing of tumor metastasis. Metastasis is defined as the capacity of tumor cells to move from the original tumor to adjacent or distant tissues and spread to other organs [2].

Transition metals, particularly multiple platinum derivatives, have been tested in clinical trials against several types of cancers and cisplatin is one of the most potent chemotherapy drugs approved for clinical practice worldwide. However, its use is limited due to severe side effects. The other two FDA-approved agents are carboplatin and oxaliplatin, while nedaplatin,

lobaplatin and heptaplatin received restricted approval for clinical use [3]. Furthermore, many non-platinum compounds have been evaluated against tumor cells. The clinical phase I trials of three ruthenium compounds: indazolium *trans*-[tetrachlorobis(1*H*-indazole)ruthenate(III)] KP1019, sodium *trans*-[tetrachlorobis(1*H*-indazole)ruthenate(III)] NKP1339 and imidazolium *trans*-[tetrachloro-(*S*-dimethylsulfoxide)(1*H*-imidazole)ruthenate(III)] NAMI-A has led to considerable interest in anticancer drugs based on this metal center [4,5]. Over the last two decades, Ru–arene complexes have become a focus of interest due to their anticancer properties [6–9]. These kind of metal complexes with monodentate or bidentate ligands showing different modes of action [10] such as apoptosis induction via DNA damage and anti-angiogenic properties [11], protein kinase inhibitors [12] protein RNase A [13] or a multi-target concept inhibit human topoisomerase IIα and covalently bind to DNA [14].

Organometallics and coordination ruthenium complexes containing well-known antifungal compounds like clotrimazole (CTZ) and ketoconazole (KTZ) have shown promising biological properties against *Leishmania major*, *Trypanosoma cruzi* [15], *Mycobacterium tuberculosis* [16] and also display antiproliferative activities on human tumor cells lines [17]. Some of these complexes present a mechanism of cell death preferentially through apoptosis. The triazole compound Fluconazole (FCZ) together with other azole compounds were evaluated against human breast adenocarcinomas MCF-7 and MDA-MB-231 and the compounds CTZ and KTZ showed induction of apoptosis, cell cycle arrest in the G1 phase, anti-migration, and anti-invasion properties [18].

We recently reported four organoruthenium complexes incorporated in the coordination sphere of ligands CTZ, KTZ or FCZ, triphenylphosphine and chloride, presenting the formulas $[RuCl(\eta^6\text{-}p\text{-cymene})(\mu\text{-FCZ})]_2[Cl]_2$ (**1**), $[RuCl(FCZ)(\eta^6\text{-}p\text{-cymene})(PPh_3)]PF_6$ (**2**), $[RuCl(CTZ)(\eta^6\text{-}p\text{-cymene})(PPh_3)]PF_6$ (**3**) and $[RuCl(KTZ)(\eta^6\text{-}p\text{-cymene})(PPh_3)]PF_6$ (**4**), which display high antiparasitic activity and ultrastructural alterations against *Leishmania amazonensis* [19]. In this work, we evaluated the ability of complexes **1**–**4** to interact with important biological targets such as human serum albumin (HSA) and DNA, as well as, their cytotoxic activity against three human tumor cell lines: Prostate (DU-145), breast (MDA-MB-231), lung (A549) and non-tumor (MRC-5 and L929). The most active ruthenium complex was selected to study the mechanism of action in the breast tumor cell line through analysis of morphology, clonogenic, migration, cell cycle and cell death assays.

2. Results and Discussion

2.1. Interaction Studies with Macro-Biological Targets: Blood Human Serum Albumin and DNA

The organoruthenium complexes were previously synthetized from $[RuCl_2(\eta^6\text{-}p\text{-cymene})]_2$ and $[RuCl_2(\eta^6\text{-}p\text{-cymene})(PPh_3)]$ by reaction with FCZ, CTZ or KTZ in methanol at different molar ratios. All complexes were characterized by usual techniques including X-ray; their chemical structures are shown in Scheme 1 [19].

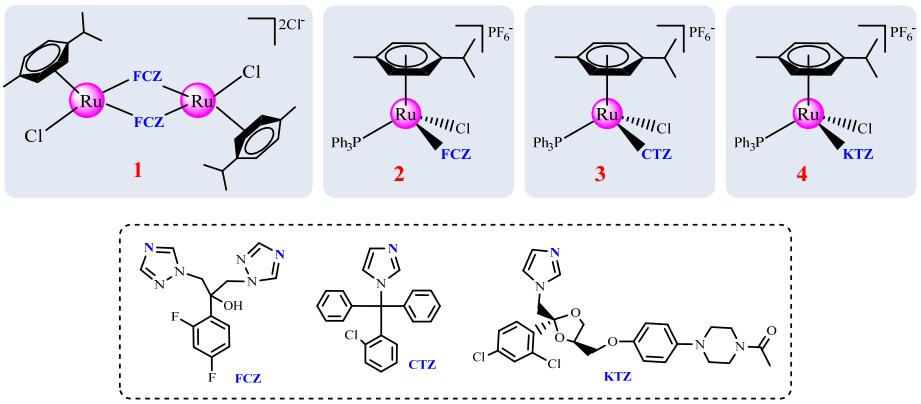

Scheme 1. Structure of organoruthenium complexes **1**–**4**.

In order to study the interaction of complexes **1–4** with blood human serum albumin (HSA), fluorescence quenching was used, which is considered the earliest and simplest method for measuring binding affinities between this protein and an organic or inorganic compound. The advantage of this technique is that it has shown a decrease in the quantum yield of fluorescence from a fluorophore induced by a variety of molecular interactions with a quencher molecule. Albumin proteins are considered to have intrinsic fluorescence due to the presence of three fluorophores: tryptophan, tyrosine and phenylalanine, the latter two contributing to its fluorescence to only a minor extent [20]. The results obtained by exciting HSA at 280 nm and recording its emission (λ_{max} = 305 nm) as a function of the concentration of complexes **2–4** are shown in Figure S1. Compound **1** does not decrease protein fluorescence intensity in the experimental conditions used, and therefore it was not possible to calculate its interaction with the protein. The Stern–Volmer quenching constant (*K*sv), binding constants (K_b), the number of binding sites (n) and thermodynamic parameters ΔH, ΔS and ΔG were calculated accordingly with the equation descripted in the supplementary material. The results show that Ksv is inversely correlated with temperature (Table 1), indicating a quenching static mechanism caused by a specific interaction between the HSA and Ru–azole complexes (**2–4**).

The values of n approximate to 1 suggest that only one reactive site exists in HSA for these Ru(II)–azole complexes. The magnitude of K_b values calculated for complexes **2–4** were between (1.78–7.90) × 10^5 M^{-1}, which suggested a moderate interaction with the HSA molecule, when compared with other metal complexes [21]. Ross et al. [22] have used the signal and magnitude of the thermodynamic parameters to interpret the nature of the interaction in a variety of host-guest systems. The negative values of ΔG support the assertion that the binding process is spontaneous. The positive ΔH and ΔS values of the interaction of all Ru(II)–azole complexes to HSA indicate that the electrostatic interactions played a major role in the binding reaction, which is allowed by the positive charge of the complexes with negative regions of the protein. Indeed, the fluorescence spectral results of two ruthenium(II) arene complexes of curcumin (O–O) analogs with the general formula [RuCl(η^6-*p*-cymene)(O–O)] indicated that they quenched the intrinsic fluorescence of HSA through static quenching mode and the thermodynamic parameters showed that Van der Waals and hydrogen bond interactions played major roles in complex stabilization [23].

Table 1. Stern–Volmer quenching constant (K_{sv}, L·mol^{-1}), bimolecular quenching rate constant (K_q, L·mol^{-1}·s^{-1}), binding constant (K_b, M^{-1}), the number of binding sites (n), ΔG (KJ·mol^{-1}), ΔH (KJ·mol^{-1}) and ΔS (J·mol^{-1}·K) values for the complex-HSA system.

Compound	T (K)	K_{sv} (10^4)	K_b (10^5)	n	ΔG	ΔH	ΔS
2	295	1.32 ± 0.06	2.35 ± 0.04	1.30	−30.35	15.73	156.12
	310	1.24 ± 0.10	1.72 ± 0.02	1.25	−31.10		
3	295	1.93 ± 0.08	5.35 ± 0.70	1.25	−32.40	38.90	241.32
	310	1.83 ± 0.03	2.50 ± 0.20	1.25	−32.04		
4	295	2.71 ± 0.04	7.90 ± 0.14	1.35	−34.30	17.70	172.90
	310	2.45 ± 0.03	5.57 ± 0.22	1.30	34.10		

The interaction of compounds **1–4** with calf thymus DNA (ct-DNA) were studied by UV–vis titration, viscosity, circular dichroism (CD) and agarose gel electrophoresis assay using procedures previous reported by us [24]. From the UV–vis titration experiments, changes in the UV–vis spectrum were clearly observed, showing an intense absorption band around 280 nm for all Ru(II)–azole complexes. After adding increasing amounts of ct-DNA to the compound, as previously reported, they showed a decrease in the intensity of the absorbance and also bathochromic shifts; however, it was not possible to calculate the binding constant because the data presented a non-linear correlation. Viscosity measurements have often been used to evaluate structural changes in the DNA helix and to determine intercalation or non-intercalation binding modes of metal complexes to DNA in solution. The ct-DNA

viscosity was constant in different complex/DNA ratios. This behavior in DNA viscosity ruled out the intercalative binding mode of the complexes to DNA.

To investigate in more detail the interaction of complexes **1–4** with ct-DNA, CD assessments were performed. The CD spectrum of ct-DNA free consists of two bands due to base stacking and to the helicity, which is a characteristic of DNA in the right-handed B form [25]. All Ru(II)–azole complexes did not induce changes in the ct-DNA CD spectrum, neither in the helicity of the negative or positive bands. Considering that, the interaction between pBR322 DNA with compound **1–4** was studied by agarose gel electrophoresis assays, observing a lower intensity of the bands corresponding to supercoiled (SC), open circular (OC) and linear (L) forms with increasing concentration of these compounds. An explanation for this result is the replacing of ethidium bromide (EB), used as staining in this assay, resulting in no fluorescent bands, even though this behavior has been reported mainly by DNA intercalation binding compounds, and it is also reported that several compounds are able to replace EB through DNA groove interaction [26,27]. For example, Hoechst 33258 (H33258), a known benzimidazole dye (not intercalator compound) binds to the minor groove of ds-DNA with a preference for adenine and thymine-rich, and its fluorescence intensity greatly increases when it is bound to DNA [28,29]. For this reason, a competitive Hoechst 33258 (H33258) displacement assay was performed by fluorescence spectroscopy. The emission spectra of the H33258-DNA adduct in the presence of increasing amounts of **1** is shown in Figure 1. The emission spectra for complexes **2–4** is shown in Figure S2.

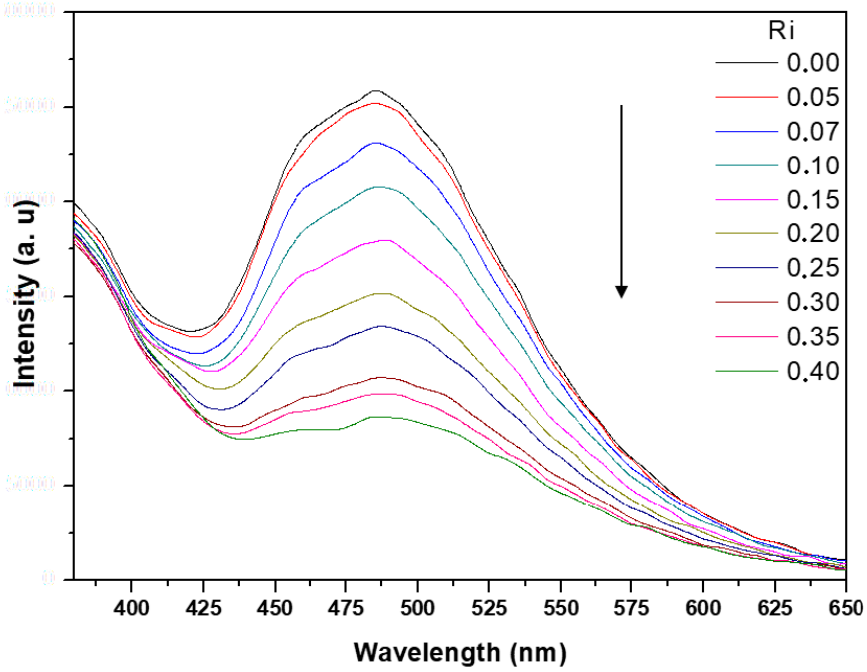

Figure 1. Hoechst 33258 (H33258) displacement assay for metal complex **1.**

A decrease in the fluorescence intensity occurred and fluorescence quenching was observed due to the release of free H33258 molecules from the H33258-DNA adduct, which suggested that **1–4** acted as minor groove binders. The K_{SV} values calculated and shown in Table 2 presented an inverse correlation with the temperature, which indicates a static quenching mechanism, initiated by an adduct formation in the ground state. The quenching efficiency shows the following trend **1** > **2** > **3** > **4**. Thus, the interaction between new complexes **1–4** and ct-DNA is probably by groove binding that is based upon intermolecular interactions, such as electrostatic and/or van der Waals attractions resulting in relatively minor changes to the structure of the double helix [30].

Table 2. Stern–Volmer quenching constant (K_{sv}, L·mol^{-1}) values for the complex-H33528 system.

	***T* (K)**	**1**	**2**	**3**	**4**
Ksv (10^4)	298	56.71 ± 0.49	39.12 ± 0.01	11.99 ± 0.38	2.76 ± 0.29
	310	32.04 ± 0.14	24.42 ± 2.57	9.71 ± 0.81	2.30 ± 0.41

In order to confirm that no covalent binding occurs between these Ru(II)–azole complexes and DNA, due to the possible lability of the chlorido ligand present in these Ru(II) complexes, two experiments were included. A reaction between complex **3** and guanosine (DNA nitrogen base) was carried out at different times. These reactions were followed by ^{1}H (Figure S3) and ^{31}P{^{1}H} NMR. No changes were observed in the NMR spectra, indicating that non-covalent binding occurred between them. The quantification of ruthenium by inductively coupled plasma optical emission spectrometry (ICP OES) of the final solution of complex **4** with ct-DNA after 24 h of incubation (see experimental section) indicated that the amount of metal bounded to DNA was 75 ± 3 nmol of Ru/mg of DNA (corresponding to 1 atom of Ru per 20 DNA base), which can be taken as evidence that no metal–DNA covalent binding is taking place. These binding levels are lower than those observed for other metal complexes with DNA covalent binding such as cisplatin [31] and other ruthenium complexes [32]. Another family of potential ruthenium–arene complexes containing dipyrrinato ligands showed electrostatic/intercalative interaction with ct-DNA and protein affinity toward bovine serum albumin (BSA) [33].

2.2. Biological Evaluations against Tumor Cell Lines

Antiproliferative assay: The ability of complexes **1**–**4** and their respective ligands to inhibit the proliferation of selected human tumor and non-tumor cell lines were determined by MTT assay (Table 3). It is worth mentioning that before performing the biological screening, the stability of the complexes was tested using the ^{31}P{^{1}H} NMR technique in DMSO or Tris–HCl solution containing 70% DMSO. After seven days, the spectra of these complexes were the same, when compared with those recorded using fresh solutions (Figure S4). The Ru(II)–azole complexes presented good activities in vitro and were also considerably more active than their free ligand in all the cell lines tested, except for compound binuclear **1,** which was not active against the tumor cells studied, and nor was the free ligand. The present organoruthenium complexes **2**–**4** showed even higher activity than some of the other reported Ru-*p*-cymene complexes containing KTZ and CTZ. The cytotoxicity of [$RuCl_2$(η^6-*p*-cymene)(L)] or [Ru(η^6-*p*-cymene)(L)(N–N)]$^{2+}$ (L = KTZ, CTZ and N–N = bipyridine, ethylenediamine) type complexes showed IC_{50} values ranging from 4 to 74 μM for KTZ and from 5 to 546 μM for CTZ, against prostate and other tumor cells [17]. It is clear from the comparison that the presence of triphenylphosphine ligand in the complexes showed a better activity profile. Additionally, it is possible to observe that imidazole (KTZ and CTZ) ruthenium derivatives are more active against tumor cells (A549 and MDA-MB-231) than the triazole (FLZ) ruthenium derivative, showing them to be more selective to these tumor cells. To continue the biological studies and investigate the mechanism of cell death in MDA-MB-231 cells, compound **3** was selected.

Cell morphology and colony formation: To investigate the effects on cell morphology, complex **3** was incubated with the MDA-MB-231 cells at different concentrations. Figure 2A depicts the effect of the treatment on the morphology. The untreated control cells appeared phenotypically as spindle-shaped, whereas the cells treated with complex **3**, especially in 0.60 and 1.20 μM, were found to be mostly spherically shaped, demonstrating damaged cell bodies, a loss of adhesion and confluence, where there was a clear concentration-response tendency. This result suggests a clear change in cell morphology induced by complex **3**. The clonogenic cell survival assay determines the ability of a cell to proliferate, thereby retaining its reproductive ability to form a large colony (>50 cells) or a clone after treatment with a cytotoxic agent. Complex **3** at a concentration of 0.06 μM inhibited the number of colonies of MDA-MB-231 and A549 cells, when compared to the control (Figure 2B,C); however, in the

MRC-5 cells, the compound did not significantly inhibit colony formation until concentration 0.6 μM, indicating the selectivity of the compound by tumor cells. The highest concentrations (0.6 μM and 6.0 μM) completely abolished the capacity of breast and lung tumor cells to form colonies. Barr et al. described the ability to inhibit the colony number in JWA-overexpressing BGC823 cells by treatment with 2.7 μM of cisplatin [34]. In the case of treatment with 1 μM and 10 μM of NAMI-A in B16F1 cells, a decrease of cell survival was reported, however no colonies were observed with cells exposed to 100 μM NAMI-A [35]. Thus, it can be concluded that compound **3** is capable of inhibiting the cell colonies more efficiently for tumor cells than non-tumor ones.

Table 3. In vitro cytotoxicity in micromolar concentrations of the complexes in tumor cells A549, DU-145, MDA-MB-231 and non-tumor cell MRC-5, L929 by 48 h.

Compound	A549	DU-145	MDA-MB-231	MRC-5	L929
1	>100	>100	>100	>100	>100
2	2.94 ± 0.73	3.90 ± 0.85	2.35 ± 0.42	2.02 ± 0.10	2.00 ± 0.16
3	0.61 ± 0.07	5.13 ± 0.98	0.63 ± 0.03	1.16 ± 0.01	1.15 ± 0.03
4	0.64 ± 0.04	4.45 ± 0.75	0.62 ± 0.02	1.09 ± 0.06	1.80 ± 0.13
Fluconazole	>100	>100	>100	>100	>100
Clotrimazole	14.47 ± 0.95	15.82 ± 0.23	10.11 ± 2.43	12.70 ± 0.65	9.74 ± 2.05
Ketoconazole	41.85 ± 2.54	47.54 ± 2.53	10.26 ± 1.04	37.50 ± 2.25	16.35 ± 0.47
Cisplatin	14.42 ± 1.45	2.33 ± 0.40	2.44 ± 0.20	23.90 ± 0.70	16.53 ± 2.38

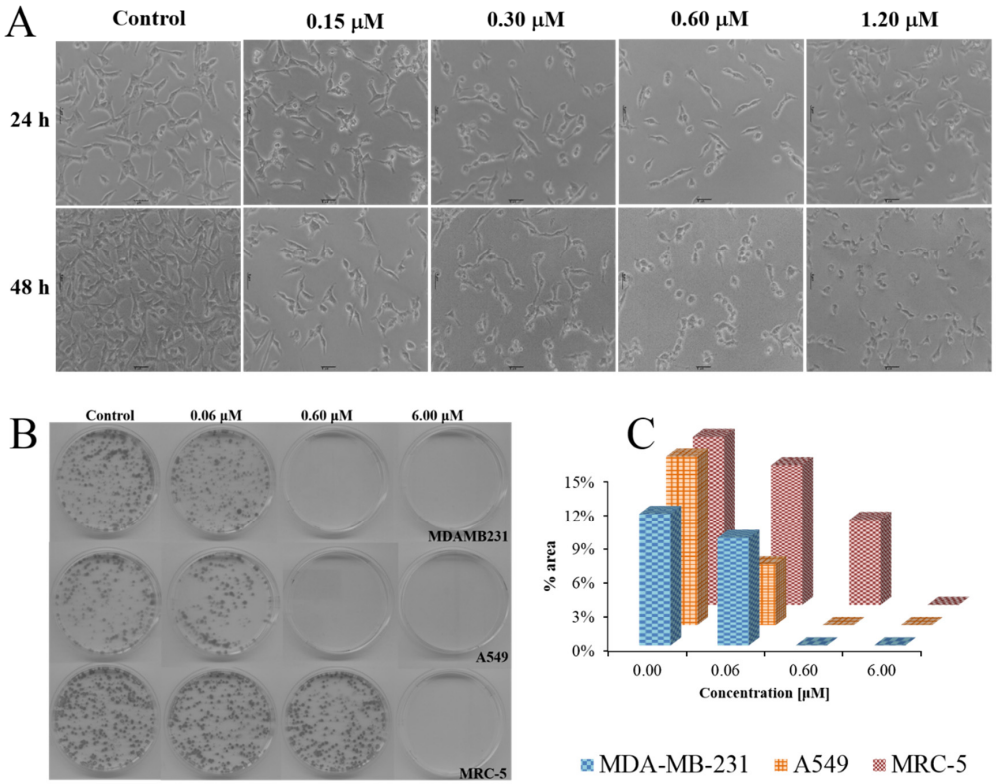

Figure 2. (**A**) Cellular Morphology of MDA-MB-231 treated with complex **3**. (**B**) Effects of complex **3** on MDA-MB-231, A549 and MRC-5 colony formation. Clonogenic assay of untreated cells (control) or treated with complex **3**. (**C**) Graph of colony area quantification.

Cell migration: Cellular migration occurs during physiological and pathological processes that play an important role in the progression of various diseases, including cancer. The Boyden chamber assay is commonly used to measure cell mobility through the PET (Polyester) transwell membrane. In vitro migration assays are necessary to understand mechanism cell migration and identify inhibitory

or stimulatory compounds [36]. To investigate the inhibition of cell migration, the invasive breast MDA-MB-231 cells were treated with different concentrations of compound **3** (lower concentrations that IC_{50} value 1.22 ± 0.07 μM, in 24 h). Moderate inhibition of the migration was observed in the MDA-MB-231 cells, as shown in Figure 3, treated with 0.15 μM and 0.30 μM of compound **3**, an average of 30% and 52% respectively, while treatment with 0.60 μM resulted in significant inhibition of migration cells (an average of 97%). Similar results described by Chen et al. demonstrated the inhibition of the migration of MDA-MB-231 cells treated with concentrations of 1.0 to 4.0 μM of $[Ru(phen)_2$-*p*-MOPIP$](PF_6)_2 \cdot 2H_2O$ (PIP = 2-phenylimidazo[4,5-*f*][1,10]phenanthroline), with $–OCH_3$ on the *p*-site substitution, a type of Ru polypyridyl complex that has been identified as a potent antimetastatic agent [37].

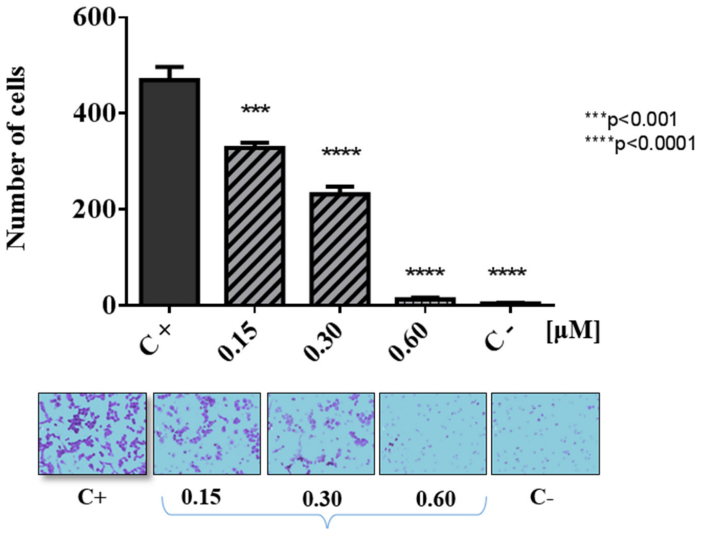

Figure 3. Effects of complex **3** on MDA-MB-231 cell migration in Boyden chambers. Up: Graph of number of cells. Down: The positive control (C+) represents migrating cells without any treatment and the negative control (C−) was cells migrating toward an FBS-free medium.

Cell cycle analysis: The ability of a compound to interfere with the distribution of cell cycle phases can provide information about their mechanism of action. To investigate the mechanism of cell division and cell cycle analysis, cytometry was performed using propidium iodide DNA staining of MDA-MB-231 cells following 24 h of treatment with 0.15, 0.30 and 0.60 μM of compound **3**. Figure 4 shows the percentage of the sub G_1, G_0/G_1, S and G_2/M phases of breast tumor cells treated with compound **3**, indicating a decrease in the number of cells in G_0/G_1 and inducing an accumulation in the number of cells in the sub-G_1 phase, similar to other ruthenium-arene complexes [33]. A small decrease of cells in the S and G_2/M phases was also observed. Identification of a sub-G1 cell population is usually related to apoptotic cells [38], which is a marker of cell death caused by apoptosis, consistent with the morphological observations described above. A large number of studies have shown that anticancer drugs can induce tumor cell apoptosis, which is the main objective of malignant tumor treatment [39].

Cell death analysis: Apoptosis occurs normally during development and aging as a homeostatic mechanism to maintain cell populations in tissues; in apoptotic cells, in addition to the morphological changes discussed above, the membrane phospholipid phosphatidylserine (PS) is translocated from the inner to the outer part of the plasma membrane, thereby exposing PS to the external cellular environment. Annexin V is a recombinant phosphatidylserine-binding protein that interacts strongly and specifically with PS residues and can be used to detect apoptosis [40]. Using a vital dye such as 7-Amino-Actinomycin (7-AAD) can identify early apoptotic cells. The extent of apoptosis for MDA-MB-231 cells caused by different concentrations of complex **3** was investigated by flow cytometry. Figure 5A shows the percentage of live cells (PE AnnexinV^-, 7-ADD^-, PI^-), cells in early apoptosis (PE AnnexinV^+, 7-ADD^-,

PI$^-$), cells in late apoptosis (PE AnnexinV$^+$, 7-ADD$^+$, PI$^+$) and necrotic cells (PE AnnexinV$^-$, 7-ADD$^-$, PI$^+$) after 24 h of exposure. The total of apoptotic cell populations in Figure 5B is expressed as the sum of percentages of early and late stages of apoptosis. These results indicate that cell death in MDA-MB-231 cells induced by compound **3** is mainly caused by apoptosis in a concentration-dependent way, in agreement with what was observed for the investigations of the cell death pathway of clotrimazole ligand, through apoptosis triggered by the displacement of key glycolytic enzymes in breast cancer cell proliferation [41], as well as for other organometallic Ru–CTZ complexes [17].

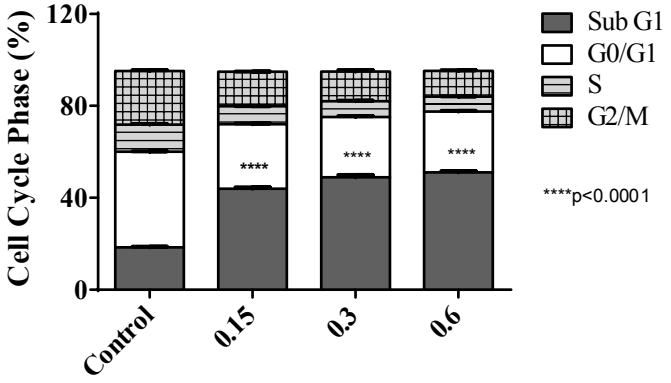

Figure 4. Effects of compound **3** on cell cycle distribution of MDA-MB-231 cells. Cell population percentages of sub-G1, G0/G1, S and G2/M phases were indicated and statistical analyses are shown as averages with indicated standard errors (n = 3).

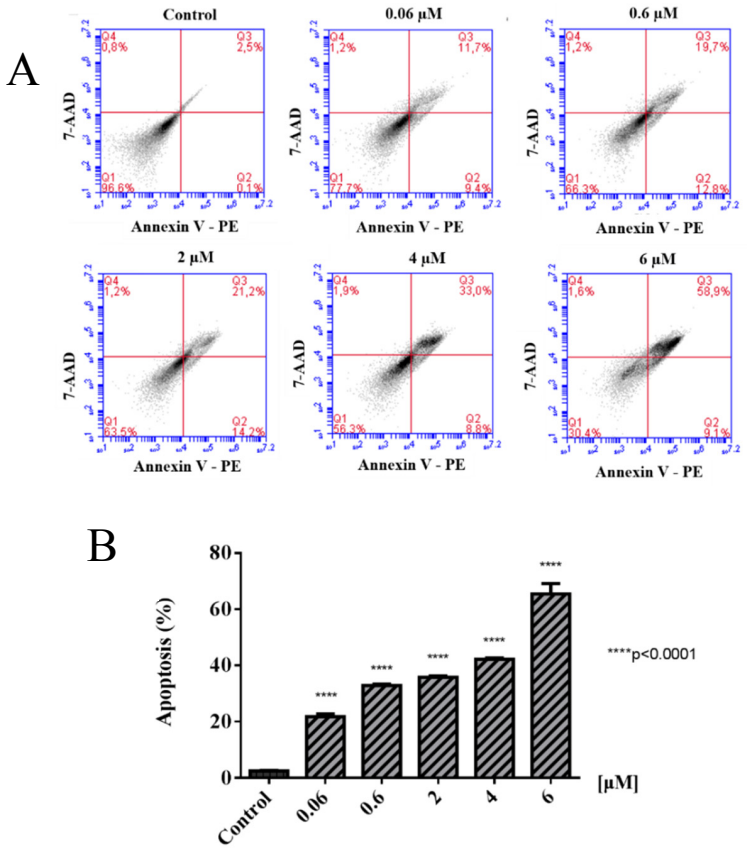

Figure 5. Effect of compound **3** on apoptosis in MDA-MB-231 tumor cells. Camptothecin was used as a positive control for apoptosis. (**A**) Cytometry analysis, the fluorescence of 7AAD is detected in the FL3-A channel and the fluorescence of PE Annexin V is detected in the FL2-A channel. (**B**) Bar chart showing percentages of apoptotic cells.

3. Materials and Methods

All the syntheses of the complexes were performed under an argon atmosphere. The ct-DNA, Hoechst 33258 and HSA were purchased from Sigma-Aldrich (St. Louis, MO, USA). Starting materials $[RuCl_2(\eta^6\text{-}p\text{-cymene})]_2$ and $[RuCl_2(\eta^6\text{-}p\text{-cymene})(PPh_3)]$ were prepared following the method described in the literature [42,43]. The organoruthenium complexes **1–4** were synthetized and characterized previously by us [19].

3.1. Biomolecules Interaction

Fluorescence measurements with HSA: HSA solutions were prepared in a Tris–HCl buffer (5 mM Tris–HCl and 50 mM NaCl, pH 7.4). A quantitative analysis of the potential interaction between the complexes and HSA was performed by fluorimetric titration (excitation at 280 nm and emission at 305 nm) monitored at different temperatures (295 and 310 K) in 96-well plates used for fluorescence assays. The HSA concentration was kept constant in all samples, while the complex concentration was increased from 100 to 0.78 μM. The experiments were carried out in triplicate on a Synergy H1 Multi-Mode Reader (BioTek, Winooski, WI, USA). The equations used to determine the constant interaction between the albumin and the studied Ru(II)–azole complexes are in the supplementary material.

Interaction studies with DNA: Hoechst 33258 displacement assays were recorded from 385 to 650 nm with an excitation wavelength of 343 nm for solutions of ct-DNA (50.0 μM), Hoechst 33258 (5.0 μM), and complexes dissolved in DMSO (0–100 μM).

DNA interaction by spectroscopic titration, viscosity, gel electrophorese, circular dichroism and reaction with guanosine were performed following the same procedure as reported previously [16].

For the determination of total metal content per mg of DNA, 10 mL of complex **4** (0.9 mM) was mixed with 10 mL of ct-DNA (4.45 mM) obtained a molar ratio of 0.2. After 24 h of incubation, the DNA was precipitated by adding 30 mL of EtOH and 1 mL of NaCl (2 M) for 10 min. At this point, the tubes were centrifuged (30 min. at 5000 rpm), the supernatant decanted, and the DNA was resuspended in water. This precipitation–resuspension cycle was repeated twice and the final DNA was solubilized in water [31]. The DNA quantification was determinate by electronic absorption measurements (Hewlett-Packard diode array-8452A, HP, Palo Alto, CA, USA). The Ru content was analyzed by IPC emission spectrometry (icap 6000 ICP OES, Thermo Fisher Scientific, Waltham, MA, USA), assisting the digestion of the sample by microwave (Berghof MW, speedwave® DIRC, Eningen, Germany). Instrument settings, data acquisition parameters and Microwave-assisted acid digestion specifications are in the supplementary material.

3.2. Biological Evaluations

Cell culture, viability and morphological observations: The cell lines were obtained from the American Type Culture Collection (ATCC), human tumor cells: A549 (lung, ATCC CCL-185), MDA-MB-231 (breast, ATCC HTB-26), DU-145 (prostate, ATCC HTB-81), non-tumor cell lines: MRC-5 (lung, ATCC CCL-171) and L929 (mouse fibroblast, ATCC CCL-1) and were cultivated under sterile conditions in Dulbecco's Modified Eagle's medium (DMEM, A549, MDA-MB-231, L929 and MRC-5) or RPMI 1640 (DU-145) supplemented with 10% of fetal bovine serum (FBS), at 37 °C in a humidified 5% CO_2 atmosphere. The growth, confluence and the morphology of the cells were observed using an inverted microscope (Nikon, T5100, Minato, Japan) and microscopic images were captured using a camera (Motic Moticam 1000, Kowloon Bay, Hong Kong, China). For antiproliferative assays, cells (1.5×10^4 cells) were seeded in flat-bottom 96-well plates, allowed to attach for 24 h prior to adding the compounds dissolved in DMSO in eight different concentrations in noneplicate. Cells were incubated at the time required, and then cell proliferation was determined by the MTT-reduction method. Briefly, 30 μL/well of MTT (1 mg/mL) was added and plates were incubated for 1−4 h at 37 °C. Finally, the formazan crystal was dissolved by adding 100 μL/well of isopropanol and quantified at 540 nm

using a multi scanner microplate absorbance reader (Labtech, LT 4000, Heathfield, England). For the morphological study, 0.8×10^5 cells/well were seeded into 12-well plates. After allowing 24 h to adhere, images of cells treated with or without compounds were taken at 0, 24 and 48 h.

Clonogenic assay: Growing tumor and non-tumor cells were harvested, counted and seeded (300 cells) into Petri dishes. Cells were allowed to grow at 37 °C in a humidified 5% CO_2 atmosphere overnight and then treated with different concentrations of the compounds **3** for 48 h. At this time point, the medium was changed without any compound. After incubation for an additional 10 days, the cells were rinsed with PBS, fixed with a solution 3:1 of methanol: acetic acid for 5 min and stained with 0.5% crystal violet for 25 min. Relative survival was calculated from the number of single cells that formed colonies of >50 cells on the 10th day. The covert area by the colonies was calculated with the Image J software.

Cell migration: The migration assay was performed using a 24-well chamber (BD Biosciences, Franklin Lakes, NJ, USA). MDA-MB-231 cells (0.5×10^5/well) were resuspended in FBS free medium and were added to the upper chamber, together with different concentrations of compound **3**. In the lower chamber, only the medium with FBS was added. The negative control contained FBS free medium. The chamber incubated for 22 h at 37 °C and 5% CO_2. Then, the cells that did not migrate to the upper surface were removed and the cells attached to the lower section were fixed with methanol, stained with toluidine blue, and washed with distilled water. Images of migrated cells were captured and counted using Image J software.

Cell cycle analysis: Cell cycle arrest was evaluated by flow cytometry. Briefly, 1.5×10^5 cells were seeded into 12-well plates and incubated for 24 h. Compound **3** (0.15, 0.30 and 0.60 μM) was added to the wells and incubated for 24 h. Then, the cells were trypsinized, collected and harvested in cold PBS and fixed in ethanol (70%) at −20 °C overnight. After this period, the cells were centrifuged; the supernatant was discarded and RNase A was added (0.2 mg·mL^{-1}) for 30 min at 37 °C. Then, the cells were stained with hypotonic fluorochrome solution (PI 5 μg·mL^{-1}, sodium citrate 0.1% and Triton-X-100 0.1%) for 1 h. Finally, the cells were analyzed by flow cytometry (Accuri C6 BD Biosciences).

Cell death analysis: The apoptosis-mediated cell death of MDA-MB-231 cells was examined by using the Annexin V-FITC Apoptosis Detection Kit (BD Biosciences), according to the manufacturer's instructions. MDA-MB-231 cells were treated with compound **3** (6.0, 4.0, 2.0, 0.60, 0.06 μM) for 24 h. In brief, 1.0×10^5 cells were harvested and washed with PBS and resuspended in 200 μL binding buffer. Next, 2.5 μL of Annexin V-FITC and 2.5 μL of PI were added. Flow cytometric analysis was performed immediately after supravital staining. The reading was performed in Accuri C6 flow cytometer (BD Biosciences) and fluorescence emitted by each dye was quantified using CellQuest software (BD Biosciences). The criteria for positivity in cells in the early stages of apoptosis were Annexin V positive and PI negative, whereas the criteria for cells in the late stages of apoptosis were Annexin V positive and PI positive.

4. Conclusions

Complexes **2**–**4** bind to HSA with moderate affinity based on the magnitude of their K_b ($1.78–7.90 \times 10^5$ M^{-1}). The thermodynamic parameters helped to understand the interaction between complexes **2**–**4** and the HSA molecule. The negative values of ΔG support the assertion that the binding process between complex/HSA is spontaneous. The positive ΔH and ΔS values of the interaction of all complexes with HSA indicate that the electrostatic interactions played a major role in the binding interaction of complex/HSA. A minor groove binding is the interaction suggested between these ruthenium(II)-azole complexes and DNA. The biological results showed that complex **2** displayed a very good activity against the tumor cells studied here. Moreover, it was demonstrated that ruthenium(II)-azole complexes **3**–**4** are significantly active in the inhibition of the proliferation of selected human tumor cells at a very low level of concentration. The phosphine used as an auxiliary ligand seems to have a significant effect on the remarkable biological activity observed for complexes

3 and **4**. Further studies will be conducted to establish a better structure–activity correlation and to identify the main target of these promising metallodrugs.

Supplementary Materials: The following are available online at http://www.mdpi.com/2304-6740/6/4/132/s1, Figure S1: Spectrofluorometric titration spectra of HSA with ruthenium compounds **2**–**4**. Figure S2: ^{1}H NMR spectrum of guanosine and complex **3** at different times (only resonances of H8, NH and NH2 are assignments). Figure S3: Hoechst 33258 (H33258) displacement assay for metal complexes **2**–**4**. Figure S4: ^{31}P{^{1}H} NMR spectrum in the mixture 70:30 DMSO: Culture medium (DMEM) of complex **3** at different times.

Author Contributions: L.C-V., K.M.O. and B.N.C. acquired and analyzed all data. L.C-V., M.R.C., M.N. and A.A.B. writing, review and editing.

Funding: Legna Colina-Vegas thanks FAPESP for her postdoctoral fellowship (grant #2016/23130-5 and 2017/23254-9).

Acknowledgments: The authors are grateful to the São Paulo Research Foundation (FAPESP), the National Counsel of Technological and Scientific Development (CNPq) and the Coordination for the Improvement of Higher Level-or Education-Personnel (CAPES) for their financial support.

Conflicts of Interest: The authors declare no conflict of interest.

References

1. *World Cancer Report 2014*; World Health Organization: Geneva, Switzerland, 2014; ISBN 9283204298.
2. Steeg, P.S. Targeting metastasis. *Nat. Rev. Cancer* **2016**, *16*, 201–218. [CrossRef] [PubMed]
3. Farrell, N.P. Multi-platinum anti-cancer agents. Substitution-inert compounds for tumor selectivity and new targets. *Chem. Soc. Rev.* **2015**, *44*, 8773–8785. [CrossRef] [PubMed]
4. Bergamo, A.; Sava, G. Ruthenium anticancer compounds: Myths and realities of the emerging metal-based drugs. *Dalton Trans.* **2011**, *40*, 7817–7823. [CrossRef] [PubMed]
5. Meier-Menches, S.M.; Gerner, C.; Berger, W.; Hartinger, C.G.; Keppler, B.K. Structure–activity relationships for ruthenium and osmium anticancer agents—Towards clinical development. *Chem. Soc. Rev.* **2018**, *47*, 909–928. [CrossRef] [PubMed]
6. Su, W.; Tang, Z.; Li, P. Development of arene ruthenium antitumor complexes. *Mini Rev. Med. Chem.* **2016**, *16*, 787–795. [CrossRef] [PubMed]
7. Zeng, L.; Gupta, P.; Chen, Y.; Wang, E.; Ji, L.; Chao, H.; Chen, Z.S. The development of anticancer ruthenium(II) complexes: From single molecule compounds to nanomaterials. *Chem. Soc. Rev.* **2017**, *46*, 5771–5804. [CrossRef] [PubMed]
8. Su, W.; Li, Y.; Li, P. Design of Ru-arene Complexes for Antitumor Drugs. *Mini Rev. Med. Chem.* **2018**, *18*, 184–193. [CrossRef]
9. Babak, M.B.; Ang, W.H. *Metallo-Drugs: Development and Action of Anticancer Agents*; Sigel, A., Sigel, H., Freisinger, E., Sigel, R.K.O., Eds.; Walter de Gruyter: Berlin, Germany, 2018; Volume 18, Chapter 6, p. 161.
10. Merlino, A. Interactions between proteins and Ru compounds of medicinal interest: A structural perspective. *Coord. Chem. Rev.* **2016**, *26*, 111–134. [CrossRef]
11. Nowak-Sliwinska, P.; van Beijnum, J.R.; Casini, A.; Nazarov, A.A.; Wagnieres, G.; van den Bergh, H.; Dyson, P.J.; Griffioen, A.W. Organometallic Ruthenium(II) Arene Compounds with Antiangiogenic Activity. *J. Med. Chem.* **2011**, *54*, 3895–3902. [CrossRef]
12. Pagano, N.; Maksimoska, J.; Bregman, H.; Williams, D.S.; Webster, R.D.; Xue, F.; Meggers, E. Ruthenium half-sandwich complexes as protein kinase inhibitors: Derivatization of the pyridocarbazole pharmacophore ligand. *Org. Biomol. Chem.* **2007**, *5*, 1218–1227. [CrossRef]
13. Hildebrandt, J.; Görls, H.; Häfner, N.; Ferraro, G.; Dürst, M.; Runnebaum, I.B.; Weigand, W.; Merlino, A. Unusual mode of protein binding by a cytotoxic π-arene ruthenium(II) piano-stool compound containing an O,S-chelating ligand. *Dalton Trans.* **2016**, *45*, 12283–12287. [CrossRef] [PubMed]
14. Kurzwernhart, A.; Kandioller, W.; Bartel, C.; Bächler, S.; Trondl, R.; Mühlgassner, G.; Jakupec, M.A.; Arion, V.B.; Marko, D.; Keppler, B.K.; et al. Targeting the DNA-topoisomerase complex in a double-strike approach with a topoisomerase inhibiting moiety and covalent DNA binder. *Chem. Commun.* **2012**, *48*, 4839–4841. [CrossRef] [PubMed]

15. Martinez, A.; Carreon, T.; Iniguez, E.; Anzellotti, A.; Sanchez, A.; Tyan, M.; Sattler, A.; Herrera, L.; Maldonado, R.A.; Sánchez-Delgado, R. Searching for new chemotherapies for tropical diseases: Ruthenium-clotrimazole complexes display high *in vitro* activity against Leishmania major and Trypanosoma cruzi and low toxicity toward normal mammalian cells. *J. Med. Chem.* **2012**, *55*, 3867–3877. [CrossRef] [PubMed]
16. Colina-Vegas, L.; Lucena Dutra, J.; Villarreal, W.; Neto, J.H.; Cominetti, M.R.; Pavan, F.; Navarro, M.; Batista, A.A. Ru(II)/clotrimazole/diphenylphosphine/bipyridine complexes: Interaction with DNA, BSA and biological potential against tumor cell lines and Mycobacterium tuberculosis. *J. Inorg. Biochem.* **2016**, *162*, 135–145. [CrossRef] [PubMed]
17. Robles-Escajeda, E.; Martínez, A.; Varela-Ramirez, A.; Sánchez-Delgado, R.A.; Aguilera, R.J. Analysis of the cytotoxic effects of ruthenium–ketoconazole and ruthenium–clotrimazole complexes on cancer cells. *Cell Biol. Toxicol.* **2013**, *29*, 431–443. [CrossRef] [PubMed]
18. Bae, S.H.; Park, J.H.; Choi, H.G.; Kim, H.; Kim, S.H. Imidazole Antifungal Drugs Inhibit the Cell Proliferation and Invasion of Human Breast Cancer Cells. *Biomol. Ther.* **2018**, *26*, 494–502. [CrossRef]
19. Colina-Vegas, L.; Coutinho, T.; Correa, R.S.; de Souza, W.; Rodrigues, J.C.F.; Batista, A.A.; Navarro, M. Antiparasitic activity and ultrastructural alterations provoked by organoruthenium complexes against Leishmania amazonensis. *New J. Chem.*, under review.
20. Lakowicz, J.R. *Principles of Fluorescence Spectroscopy*, 3rd ed.; Springer: New York, NY, USA, 2006; ISBN 978-0-38-746312-4.
21. Sun, J.; Huang, Y.; Zheng, C.; Zhou, Y.; Liu, Y.; Liu, J. Ruthenium (II) complexes interact with human serum albumin and induce apoptosis of tumor cells. *Biol. Trace Elem. Res.* **2015**, *163*, 266–274. [CrossRef]
22. Ross, D.; Subramanian, S. Thermodynamics of protein association reactions: Forces contributing to stability. *Biochemistry* **1981**, *20*, 3096–3102. [CrossRef]
23. Huang, S.; Peng, S.; Zhu, F.; Lei, X.; Xiao, Q.; Su, W.; Liu, Y.; Huang, C.; Zhang, L. Multispectroscopic investigation of the interaction between two ruthenium(II) arene complexes of curcumin analogs and human serum albumin. *Biol. Trace Elem. Res.* **2016**, *169*, 189–203. [CrossRef]
24. Colina-Vegas, L.; Luna-Dulcey, L.; Plutín, A.M.; Castellano, E.E.; Cominetti, M.R.; Batista, A.A. Half sandwich Ru(II)-acylthiourea complexes: DNA/HSA-binding, anti-migration and cell death in a human breast tumor cell line. *Dalton Trans.* **2017**, *46*, 12865–12875. [CrossRef] [PubMed]
25. Bishop, G.R.; Chaires, J.B. Characterization of DNA structures by circular dichroism. *Curr. Protoc. Nucleic Acid Chem.* **2003**, *11*, 7–11. [CrossRef]
26. Han, M.J.; Duan, Z.M.; Hao, Q.; Zheng, S.Z.; Wang, K.Z. Molecular Light Switches for Calf Thymus DNA Based on Three Ru(II) Bipyridyl Complexes with Variations of Heteroatoms. *J. Phys. Chem. C* **2007**, *111*, 16577–16585. [CrossRef]
27. Fu, X.B.; Liu, D.D.; Lin, Y.; Hu, W.; Mao, Z.W.; Le, X.Y. Water-soluble DNA minor groove binders as potential chemotherapeutic agents: Synthesis, characterization, DNA binding and cleavage, antioxidation, cytotoxicity and HSA interactions. *Dalton Trans.* **2014**, *43*, 8721–8737. [CrossRef] [PubMed]
28. Sabnis, R.W. *Handbook of Biological Dyes and Stains: Synthesis and Industrial Applications*, 1st ed.; Wiley: New York, NY, USA, 2010; ISBN 978-0-47-040753-0.
29. Fornander, L.H.; Wu, L.; Billeter, M.; Lincoln, P.; Nordeń, B. Minor-Groove binding drugs: Where is the second Hoechst 33258 molecule? *J. Phys. Chem. B* **2013**, *117*, 5820–5830. [CrossRef] [PubMed]
30. Pages, B.J.; Ang, D.L.; Wrightb, E.P.; Aldrich-Wright, A.R. Metal complex interactions with DNA. *Dalton Trans.* **2015**, *44*, 3505–3526. [CrossRef] [PubMed]
31. Navarro, M.; Castro, W.; Higuera-Padilla, A.R.; Sierraalta, A.; Abad, M.J.; Taylor, P.; Sánchez-Delgado, R.A. Synthesis, characterization and biological activity of *trans*-platinum(II) complexes with chloroquine. *J. Inorg. Biochem.* **2011**, *105*, 1684–1691. [CrossRef]
32. Frik, M.; Martínez, A.; Elie, B.T.; Gonzalo, O.; de Mingo, D.R.; Sanau, M.; Sanchez-Delgado, R.A.; Sadhukha, T.; Prabha, S.; Ramos, J.W.; et al. *In vitro* and *in vivo* Evaluation of water-soluble iminophosphorane ruthenium(II) compounds. A potential chemotherapeutic agent for triple negative breast cancer. *J. Med. Chem.* **2014**, *57*, 9995–10012. [CrossRef]
33. Gupta, K.R.; Kumar, A.; Paitandi, R.P.; Singh, R.S.; Mukhopadhyay, S.; Verma, S.P.; Dasb, P.; Pandey, P.S. Heteroleptic arene Ru(II) dipyrrinato complexes: DNA, protein binding and anti-cancer activity against the ACHN cancer cell line. *Dalton Trans.* **2016**, *45*, 7163–7177. [CrossRef]

34. Barr, M.P.; Gray, S.G.; Hoffmann, A.C.; Hilger, R.A.; Thomale, J.; O'Flaherty, J.D.; Fennell, D.A.; Richard, D.; O'Leary, J.J.; O'Byrne, K.J. Generation and characterization of cisplatin-resistant non-small cell lung cancer cell lines displaying a stem-like signature. *PLoS ONE* **2013**, *8*, e54193. [CrossRef]
35. Bicek, A.; Turel, I.; Kanduser, M.; Miklavcic, D. Combined therapy of the antimetastatic compound NAMI-A and electroporation on B16F1 tumour cells *in vitro*. *Bioelectrochemistry* **2007**, *71*, 113–117. [CrossRef] [PubMed]
36. Chen, H.C. Cell Migration. In *Developmental Methods and Protocols*, 1st ed.; Guan, J.L., Ed.; Humana Press: Totowa, NJ, USA, 2005; pp. 15–22. ISBN 978-1-59-259860-1.
37. Cao, W.; Zheng, W.; Chen, T. Ruthenium Polypyridyl Complex Inhibits Growth and Metastasis of Breast Cancer Cells by Suppressing FAK signaling with Enhancement of TRAIL-induced Apoptosis. *Sci. Rep.* **2015**, *5*, 9157. [CrossRef] [PubMed]
38. Huang, X.; Halicka, H.D.; Traganos, F.; Tanaka, T.; Kurose, A.; Darzynkiewicz, Z. Cytometric assessment of DNA damage in relation to cell cycle phase and apoptosis. *Cell Prolif.* **2005**, *38*, 223–243. [CrossRef] [PubMed]
39. Elmore, S. Apoptosis: A review of programmed cell death. *Toxicol Pathol.* **2007**, *35*, 495–516. [CrossRef] [PubMed]
40. Schutte, B.; Nuydens, R.; Geerts, H.; Ramaekers, F. Annexin V binding assay as a tool to measure apoptosis in differentiated neuronal cells. *J. Neurosci. Methods* **1998**, *86*, 63–69. [CrossRef]
41. Glass-Marmor, L.; Morgenstern, H.; Beitner, R. Calmodulin antagonists decrease glucose 6-bisphosphate, fructose 6-bisphosphate, ATP and viability of melanoma cells. *Eur. J. Pharmacol.* **1996**, *313*, 265–271. [CrossRef]
42. Bennett, M.A.; Huang, T.N.; Matheson, T.W.; Smith, A.K. (η^6-Hexamethylbenzene) ruthenium Complexes. *Inorg. Synth.* **1982**, *21*, 74–78. [CrossRef]
43. Hodson, E.; Simpson, S.J. Synthesis and characterization of [(η^6-cymene)Ru(L)X2] compounds: Single crystal X-ray structure of [(η^6-cymene)Ru(P{OPh}$_3$)Cl$_2$] at 203 K. *Polyhedron* **2004**, *23*, 2695–2707. [CrossRef]